

# SEISMIC ACTIVITY-RELATED ANOMALY DETECTION IN SOIL RADON EMANATION

*Suleyman Baykut<sup>1</sup>, Tayfun Akgul<sup>1</sup>, and Sedat Inan<sup>2</sup>*

<sup>1</sup>Department of Electronics and Communications Engineering, Istanbul Technical University, Istanbul, Turkey.

<sup>2</sup>TUBITAK - Marmara Research Center, Earth and Marine Sciences Institute, Gebze, Kocaeli, Turkey.

Phone: + (90) 212 285 3568, Fax: + (90) 212 285 3679

E-mail: baykut@itu.edu.tr, tayfunakgul@itu.edu.tr, sedat.inan@mam.gov.tr

## ABSTRACT

*Soil Radon Emanation* has been continuously monitored along with other geophysical measurements in the seismically active Marmara region of Turkey over the past ten years for understanding the pre-earthquake crustal deformation. In this paper, radon gas emanation time series are decomposed into intrinsic (characteristic) modes via *Empirical Mode Decomposition (EMD)* and the relationship between seismic activities and radon gas emanation is investigated. A statistical model of gas emanation is discussed. Also, observation of the atmospheric effects as daily-quasi-periodic fluctuations (which may sometimes dominate the recordings) is demonstrated and a signal-adaptive periodicity removal process based on the EMD method is used for robust processing. The results for both seismic and a-seismic time intervals and a short discussion on how the analysis of radon gas data can be used as a precursor of seismic activity is presented.

## 1. INTRODUCTION

In Turkey, soon after the destructive Izmit earthquake of 17 August 1999 with magnitude of  $M_w=7.4$ , along with various other seismic observations, the soil radon gas activity has been systematically monitored since 2002 in the Marmara Region (NW Turkey) covering an area of 40 000 km<sup>2</sup>; by cooperation of TUBITAK - Earth and Marine Science Institute and Istanbul Metropolitan Municipality. Since 1960s, many studies have been conducted for the search of earthquake precursors [1-5 and references therein]. Although so far it seems that there are no reliable precursors preceding large earthquakes [6], there are reports of measurements of the temporal variation of soil radon that could be related to seismic and volcanic activity ([3, 7-16] among many others). Recent studies show that soil radon gas emanation data may provide insight on temporal variation of soil gas in porous and permeable part of the shallow crust of the earth. For example, some of the observed anomalies in the soil radon emanation data, such as an abrupt change in the amplitude, can be related to seismic activities.

In this study, radon emanation data from various stations (with and without seismic activity in the vicinity of the sensor) are decomposed into intrinsic modes (characteristic components) having different frequency bands. Data-adaptive *Empirical Mode Decomposition (EMD)* is used to

extract these “physically meaningful” characteristic components. Then high-frequency and low-frequency components of the data are investigated in order to observe possible anomalies related to the seismic activity or other effects such as variations in temperature and/or precipitation. Meteorological effects are observed as daily pseudo-periodic components in soil radon data. It is shown that pseudo-periodic atmospheric effects can be easily removed by subtracting the corresponding periodic intrinsic modes from the overall data [17]. Furthermore, a discussion about the distribution of the radon gas emanation data is provided for both seismic and a-seismic periods.

## 2. BACKGROUND

### 2.1 Soil Radon Emanation Data

The locations of the soil radon monitoring stations in Marmara region of Turkey are shown in the map in Fig. 1. The soil radon gas emanation is measured via silicon detector based alpha-particle counting tools (Alpha-meter) [11]. At each location one radon sensor is used at approximately one meter soil depth. Meteorological data are obtained from nearby meteorology stations on the weather underground web site. The alpha particles emitted by radon gas are counted in 15 minute intervals and recorded into the memory of the device. In this paper, data collected at *Armutlu*, *Gönen* and *Efteni (Düzce)* stations are studied.

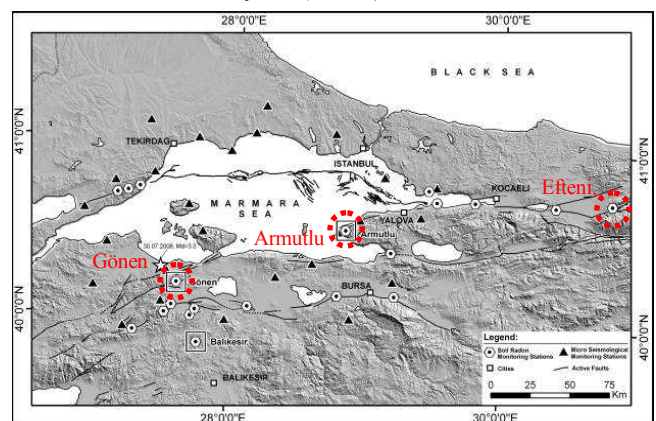


Figure 1 – Soil radon gas monitoring stations (white circles) in Marmara region of Turkey (*Armutlu*, *Gönen* and *Efteni (Düzce)* stations are marked by red circles.)

## 2.2 Empirical Mode Decomposition

Empirical mode decomposition is a data-adaptive, easy and powerful signal decomposition method which is shown to be convenient in the analysis of non-stationary signals [18-20]. EMD iteratively decomposes the signal into several Intrinsic Mode Functions (IMF). IMFs are considered as the characteristic (physically meaningful) modes of the signal in different frequency regions which catch local oscillations within the signal. The method does not need any a-priori defined basis. In “sifting” process, which is the main procedure of the method, fast oscillations in the signal are isolated from the slow ones iteratively. The first IMF which consists of locally highest frequency components is obtained after the first sifting. This IMF is subtracted from the signal and the sifting procedure is repeated using remainder signal to get the next IMF. Iterations are run until some stopping criteria are fulfilled [19]. IMFs are zero-mean signals having the same number of zero-crossing points and local extrema (minimum and maximum) points (or differ by 1 at most.) The signal,  $x(t)$ , can perfectly be constructed by summing up the IMFs, i.e.,

$$x(t) = \sum_{k=1}^{K-1} d_k(t) + r(t) \quad (1)$$

Here,  $d_k(t)$  is the  $k^{\text{th}}$  IMF.  $r(t)$  is the residual signal which can be considered as the last ( $K^{\text{th}}$ ) IMF. Each IMF covers the lower frequency regions locally in time-frequency plane than the previous IMF. For wide-band signals, EMD behaves like a dyadic filter bank [19, 20].

## 3. ANALYSIS AND OBSERVATIONS

EMD algorithm is applied to the selected parts of the radon data. Then the IMFs are recombined to construct the high-frequency (noise), low-frequency (trend) and daily quasi-periodic parts of the time series.

### 3.1 Seismicity-related Radon Emanation Data

It is known that soil radon emanation is influenced by the seismic activities around the measurement area [16, 21]. Gas release shows a positive anomaly (an increase in the gas concentration) prior to earthquakes with a magnitude of  $M > 4$  [21] (up to 100 km in distance from the measurement station.) In this paper three examples are provided in order to show the seismicity related anomalies. In Fig. 2, temporal variation of soil radon gas at *Armutlu* station between 1<sup>st</sup> Sept. – 31<sup>st</sup> Oct. 2004 is shown. On the 29<sup>th</sup> September at 18:42 (Turkish Standard Time -TST), an earthquake (EQ) with a magnitude of  $M = 4.0$  has occurred at distance of ~50 km to the measurement station. The time of the EQ is shown as a vertical line on the same plot. As reported in [21], pre-earthquake anomaly is detected as an increase in radon values. To magnify the effect, the data is automatically decomposed into 12 IMFs by EMD algorithm. The first 6 IMFs and the last 6 IMFs are combined to reconstruct the high-frequency (Fig.3-a) and very low-frequency (Fig.3-b) components of the time series, respectively. The latter can be considered as the local mean (trend/baseline) of the data. It is clear in Fig. 3-b that the local mean of the radon data in-

crease prior to the EQ. There is a sharp decrease after the EQ and the local mean drops to a smaller baseline afterwards compared to the one during the pre-EQ time period. The variance of the HF-component is also increasing prior to the EQ. This can be seen in Fig.4, where the short-time variances of the HF-component are shown. Here the window size is set to 2 days with a 1-day overlap.

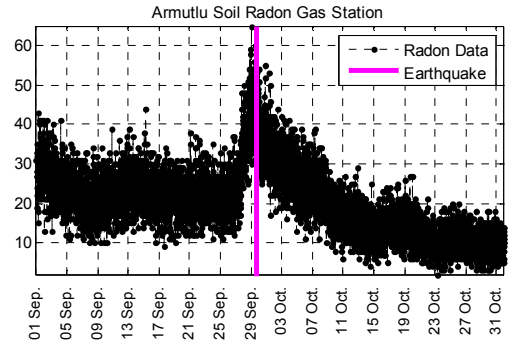


Figure 2 – Temporal variation of soil radon gas at *Armutlu* station between 1<sup>st</sup> Sept. – 31<sup>st</sup> Oct. 2004 (As seen in [21]). (Vertical line on the 29<sup>th</sup> Sept. 18:42 (TST) shows the time of EQ with  $M=4.0$ ).

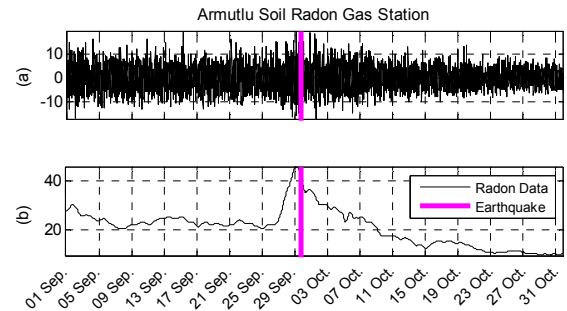


Figure 3 – (a) High- and (b) low-frequency components of the *Armutlu* data given in Fig.2.

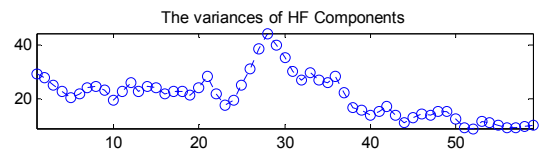


Figure 4 – The variances of the HF components of *Armutlu* data given in Fig.3-a (window length is set to 2 days with 1 day overlap).

The next example shown in Fig.5 is the radon data collected at *Gönen* station between 19<sup>th</sup> April and 25<sup>th</sup> April 2009. An EQ occurred with a magnitude of  $M = 2.7$  on the 22<sup>nd</sup> April, 2009 19:24 (TST) within 20 kilometers to the *Gönen* measurement station. This EQ is marked as a vertical line on the same plot. The magnitude of the EQ is smaller than the previous one. However, since the epicenter of the EQ is very close to the station, the pre-earthquake stress buildup apparently affects the radon gas emanation, again as an increase in the data baseline. 5-days-long radon data is decomposed into 8 IMFs by EMD and the HF and LF components are constructed by combining the first 4 and the last 4 IMFs (Fig.6). While there was no obvious variation at the HF component levels, the LF component (baseline) shows a rapid increase and a rapid decay within 24 hours having the EQ in the middle.

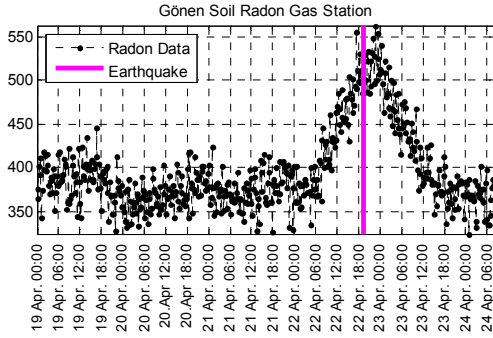


Figure 5 – Temporal variation of soil radon gas at *Gönen* station between 19<sup>th</sup> and 25<sup>th</sup> April 2009. (Vertical line on the 22<sup>nd</sup> April, 2009 19:24 (TST) shows the time of EQ with  $M=2.7$ ).

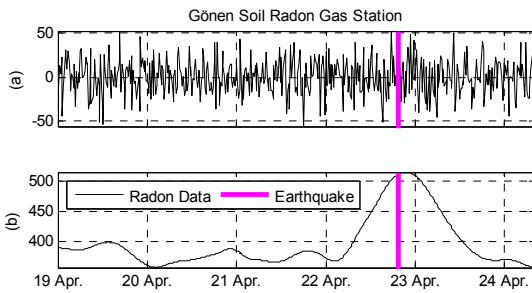


Figure 6 – (a) High- and (b) low-frequency components of the *Gönen* data given in Fig.5.

The last example is taken from *Efjeni (Düzce)* station. This time, a longer period (a full year of 2003) data is provided in Fig.7 to show the regional seismicity related variations. The EQs occurred in the area with a magnitude greater than 4.0 are also marked as vertical lines on the plot.

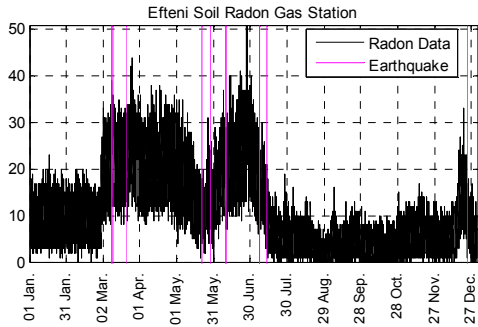


Figure 7 – Temporal variation of soil radon gas at *Efjeni (Düzce)* station for a full year of 2003 (Vertical lines corresponds to the times of EQs occurred in the area with a  $M \geq 4.0$ ).

The dates, the magnitudes ( $M$ ) and the distances ( $d$ ) of the EQs around this monitoring station are as follows; 8<sup>th</sup> March 13:18 ( $M=4.0$ ,  $d \sim 50$ km); 9<sup>th</sup> March 21:01 ( $M=4.1$ ,  $d \sim 50$ km), 20<sup>th</sup> March 14:25 ( $M=4.5$ ,  $d \sim 50$ km); 21<sup>st</sup> May 11:21 ( $M=4.5$ ,  $d \sim 15$ km); 28<sup>th</sup> May 02:25 ( $M = 4.0$ ,  $d \sim 15$ km); 9<sup>th</sup> June 20:44 ( $M = 5.1$ ,  $d > 200$ km); 9<sup>th</sup> June 20:47 ( $M = 4.1$ ,  $d > 200$ km); 6<sup>th</sup> July 22:10 ( $M=5.3$ ,  $d > 200$ km); 6<sup>th</sup> July 23:10 ( $M=4.9$ ,  $d > 200$ km); 13<sup>th</sup> July 08:09 ( $M=4.0$ ,  $d > 200$ km); and 23<sup>rd</sup> December 14:23 ( $M=4.8$ ,  $d \sim 140$ km). Note that, there were also several small-magnitude EQs in the vicinity of the measurement station appeared as aftershocks. Whole data is

decomposed into IMFs. Then HF and LF components are constructed as in Fig.8. The baseline data shows an abrupt increase prior to the first 2 EQs. In the seismically active time period (between March and July) the baseline (local mean) of the radon gas emanation proceeds at higher values compared to the pre-EQ and post-EQ (quite) periods. Time-varying variance of the HF-component is investigated using sliding windows having length of 2 days with a 1-day overlap. The variances of the windows are given in Fig.9. It is clear in the figure that the variance of the HF-component is also having greater values during seismically active period compared to the quite terms. The very last EQ resulted in a narrow peak at both HF and LF-components lasting about a week.

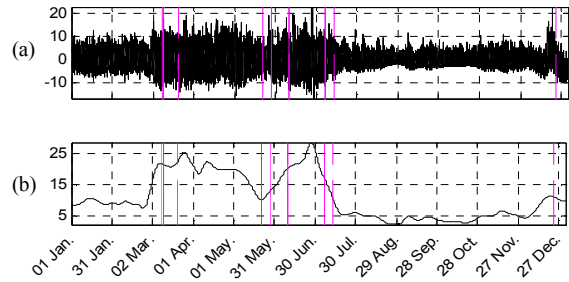


Figure 8 – (a) High- and (b) low-frequency components of the *Efjeni (Düzce)* data given in Fig.7.

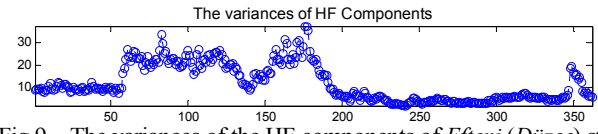


Fig.9 – The variances of the HF components of *Efjeni (Düzce)* station given in Fig.8-a (2-day long windows with a 1 day overlap).

### 3.2 Atmospheric Effects

It is known that radon gas emanation is affected by several meteorological phenomena such as pressure, temperature, precipitation, etc. [17, 22-28]. Among meteorological parameters rainfall is known to adversely affect radon emanation. During heavy rainfall radon emanation in soil is suppressed. Effect of variation in atmospheric pressure is not as clear. Normally negative correlation is expected between atmospheric pressure and soil radon data if the soil is permeable (e.g., crack formations during droughtiness or sand-size grain dominated soil); this seemingly negative correlation cease to exist when the soil is relatively impermeable [21]. Most dominant effects appear as (quasi) periodical components due to seasonal and/or diurnal variations of precipitation, pressure and temperature changes. Heavy precipitation during winter causes very high moisture in soil and this retards radon emanation throughout winter months [15]. On the other hand, temperature is known to be the main reason for daily-periodicity in radon gas emanation. Usually in summer when the soil is dry and cracked, air penetrates into the deeper parts and thus visible quasi-periodic behavior exists as a result of diurnal variations in temperatures [17]. This periodicity may cover the other possible seismicity effects and must be removed from the data. Here EMD is used to identify and extract the pseudo-periodic component from the

data as suggested in [17]. First the data is decomposed into several IMFs. Then the IMF that has nearly 1-day-long period is removed and the remainders are summed up to construct the clean data. A 5-day long (26<sup>th</sup> – 31<sup>st</sup> July) example data measured at *Gönen* station is given in Fig.10 where dominant daily periodicity is visible. The corresponding IMFs are given in Fig. 11. The 5<sup>th</sup> IMF corresponds to the daily-periodic components. After removing the 5<sup>th</sup> IMF daily-periodicity (Fig.12-b) periodicity-free data can be obtained as in Fig. 12-c.

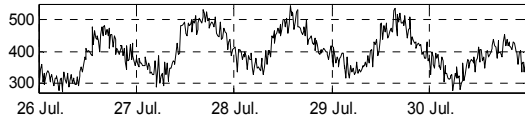


Figure 10 – Temporal variation of soil radon gas at *Gönen* station between 26<sup>th</sup> and 31<sup>st</sup> July.

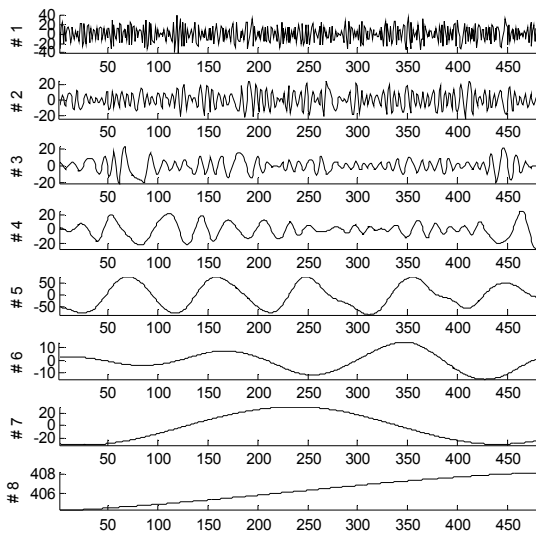


Figure 11 –IMFs of the *Gönen* data given in Fig. 10.

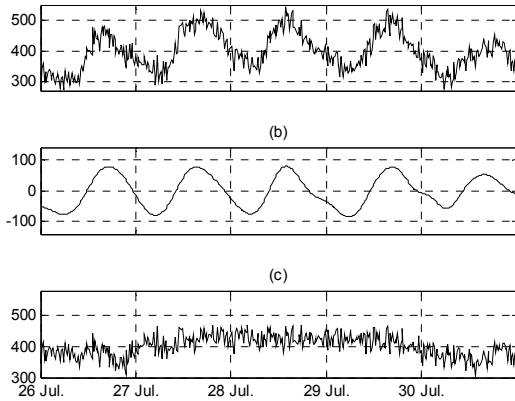


Figure 12 – (a) *Gönen* data, (b) Daily quasi-periodic effect (5<sup>th</sup> IMF), and (c) clean data without periodicity.

### 3.3 Statistical Characterization of the Data

In order to investigate the distribution of the radon gas emanation both for seismic and a-seismic periods, two set of data are chosen from *Efteni* station measurements given in Fig.7. This monitoring site is situated within the brecciated zone of an active fault [21]. “1<sup>st</sup> March – 1<sup>st</sup> May” phase is selected as “seismic period” where several EQs with  $M > 3$

were recorded, whereas “1<sup>st</sup> September – 1<sup>st</sup> November” phase is selected as “a-seismic period” where no seismic event were present. Soil radon data corresponds to the radon intensity level around the sensor by counting the alpha particles released by the radioactive decay of radon over a 15-min fixed interval. Since the process can be considered as a count-process if there are no external effects, its distribution can be modeled by Poisson distribution [29]. Another phenomenon that affects the intensity of the gas is upward transport of the gas through soil from the source to the sensor. This movement depends on the physical characteristics of the soil such as fractures, porosity, permeability, etc. which may be modeled as 3D random walk [21]. Assuming that the radon has a particle behavior with random moves over an irregular ground path then, such movement results in Rayleigh-type exponential probability density function (pdf) as suggested for any random-walk behavior [29]. As a result, for overall radon gas data one can expect to observe Rayleigh-type and/or Poisson-type (or perhaps combination of both) distribution functions.

Rayleigh, Poisson and Gaussian pdfs are fitted to the histogram of the mentioned data segments using maximum likelihood method. In Fig.13-a, the normalized histogram of the a-seismic-period data is plotted with Poisson and Rayleigh pdf fits. The minimum fit error is obtained for Poisson pdf (approximately 20 times smaller than the Gaussian fit error). In Fig.13-b, the normalized histogram of the seismic-period data is plotted with best probability density function fit which is Gaussian pdf in this case. Here, the Gaussian fit error is about 3 times smaller compared to the Poisson pdf fit error. This observation suggests that the distribution converges to Gaussian prior to seismic activity. One can conclude that, during earthquake building process (e.g., accumulation of critical crustal stress), micro-fracturing of the rock is enhanced leading to increasing paths for radon migration forcing the distribution towards Gaussian (law of large numbers). The same behavior is observed for all other stations.

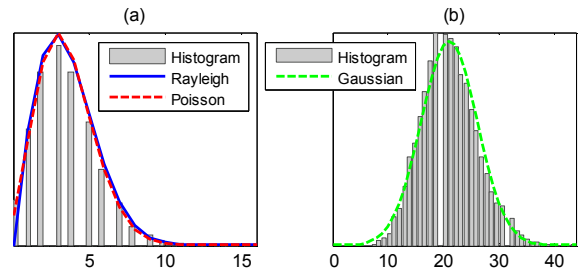


Figure 13 – Histograms and fitted pdf's for a-seismic (a) and seismic (b) periods.

## 4. CONCLUSIONS

Soil radon data probably contains pre-earthquake signals; however, in soil environment emanation of radon may be strongly influenced by atmospheric variations. In case these effects can be detected and removed from the data via EMD method as described in the paper, pre-earthquake related anomalies in the soil radon may become more apparent and more reliable. It is observed that the soil radon emanation increases in the pre-earthquake phase. This anomaly is ap-

parent in both baseline (LF components), and high frequency components obtained by EMD. The studies of the noise characteristics of radon data can be practical and useful for anomaly detection that may be interpreted as precursors to seismic activity. Finally, it has been shown that during a-seismic (quiescence) periods, the soil radon data show Rayleigh-type and/or Poisson-type (or combination of both) distributions. However, during earthquake phase the radon data distribution tends to Gaussian or multiple (mixture) distributions.

## REFERENCES

- [1] H. Wakita, "Geochemical challenge to earthquake prediction," *Proceedings of the National Academy of Sciences, USA*, vol. 93, pp. 3781-3786, 1996.
- [2] C. Y. King, "Gas geochemistry applied to earthquake prediction: A Review," *Journal of Geophysical Research*, vol. 91, pp. 12269-12281, 1986.
- [3] J. Toutain, J. Baubron, "Gas geochemistry and seismotectonics: a review," *Tectonophysics*, vol. 304, no. 127, pp. 1-27, 1999.
- [4] L. Claesson, A. Skelton, C. Graham, C. Dietl, M. Moerth, P. Torssander, I. Kockum, "Hydrogeochemical changes before and after a major earthquake," *Geology*, vol. 32, pp. 641-644, 2004.
- [5] J. Hartmann, J. K. Levy, "Hydrogeological and gasgeochemical earthquake precursors – A review for application," *Natural Hazards*, vol. 34, pp. 279-304, 2005.
- [6] W. L. Turcotte, "Earthquake prediction," *Annual Review Earth and Planetary Sciences*, vol. 19, pp. 263-281, 1991.
- [7] G. Sultankhodhaev, "Earthquake prediction," *UNESCO, Paris*, pp. 181-191, 1984.
- [8] H. Virk, B. Singh, "Radon anomalies in soil gas and groundwater as earthquake precursor phenomena," *Tectonophysics*, vol. 227, pp. 215-224, 1993.
- [9] H. Wakita, Y. Nakamura, Y. Sano, "Short-term and intermediate term geochemical precursors," *Pure and Applied Geophysics*, vol. 125, pp. 267-278, 1988.
- [10] J. King, Y. Koizumi, Y. Kitagawa, "Hydrogeochemical anomalies and the 1995 Kobe earthquake," *Science*, vol. 269, pp. 38-39, 1995.
- [11] D. Thomas, J. C. D. Holdford, "Experimental design for soil gas radon monitoring," *Journal of Radio-analytical and Nuclear Chemistry*, vol. 161, pp. 313-323, 1992.
- [12] L. L. Chyi, C. Y. Chou, T. F. Yang, C. H. Chen, "Continuous radon measurements in faults and earthquake precursor pattern recognition," *Western Pacific Earth Sciences*, vol.1, no.2, pp. 227-246, 2001.
- [13] C. Martin-Luis, M. Quesada, A. Darwich, J. Dela Nuez, J. Coello, "A new strategy to measure radon in an active volcanic island (Tenerife, Canary Islands)," *Environmental Geology*, vol. 43, pp. 72-78, 2002.
- [14] J. Planinic, V. Radolic, B. Vukovic, "Radon as an earthquake precursor," *Nuclear Instruments and Methods in Physics Research A*, vol. 530, pp. 568-574, 2004.
- [15] S. Inan, K. Ertekin, C. Seyis, Ş. Şimşek, F. Kulak, A. Dikbaş, O. Tan, S. Ergintav, R. Çakmak, A. Yörük, M. Çergel, H. Yakan, H. Karakuş, R. Saatçılar, Z. Akçiğ, Y. Iravul, B. Tüzel, "Multi-disciplinary earthquake researches in western Turkey: Hints to select sites to study geochemical transients associated to seismicity," *Acta Geophysica*, vol. 58, pp. 767-813, DOI: 10.2478/s11600-010-0016-7, 2010.
- [16] S. Inan, C. Seyis, "Soil radon observations as possible earthquake precursors in Turkey," *Acta Geophysica*, vol. 58, pp. 828-837, doi:10.2478/s11600-010-0010-0, 2010.
- [17] S. Baykut, T. Akgül, S. Inan, C. Seyis, "Observation and Removal of Daily Quasi-Periodic Components in Soil Radon Data," *Radiation Measurements*, doi.10.1016/j.radmeas.2010.04.002, April 2010.
- [18] N.E. Huang, Z. Shen, S. R. Long, M. L. Wu, H. H. Shih, Q. Zheng, N. C. Yen, C. C. Tung, H. H. Liu, "The empirical mode decomposition and the Hilbert spectrum for nonlinear and non-stationary time series analysis," *Proceedings of the Royal Society of London A*, vol. 454, pp. 903-995, 1998.
- [19] G. Rilling, P. Flandrin, P. Goncalves, "On empirical mode decomposition and its algorithms," *IEEE-EURASIP Workshop on Nonlinear Signal and Image Processing NSIP-03*, Grado, 2003.
- [20] Z. Wu, N. Huang, "A study of the characteristics of white noise using the empirical mode decomposition method," *Proceedings of the Royal Society of London A*, vol. 460, pp. 1597-1611, 2004.
- [21] S. Inan, T. Akgül, C. Seyis, R. Saatçılar, S. Baykut, S. Ergintav, M. Baş, "Geochemical monitoring in the Marmara region (NW Turkey): A search for precursors of seismic activity," *Journal of Geophysical Research*, vol. 113, B03401, 2008.
- [22] A. Tanner, "Radon migration in the ground: A supplementary review," *Proc. of the Natural radiation Environment, U.S. Dpt. of Energy Report*, vol. 111, pp. 5-56, 1980.
- [23] J. Washington, A. Rose, "Regional and temporal relations of radon in soil gas to soil temperature and moisture," *Geophysical Research Letters*, vol. 17, pp. 829-832, 1990.
- [24] R. Winkler, F. Ruckerbauer, K. Bunzl, "Radon concentration in soil gas: a comparison of the variability resulting from different methods, spatial heterogeneity and seasonal fluctuations," *The Science of the Total Environment*, vol. 272, pp. 273-282, 2001.
- [25] M. Finkelstein, L. V. Eppelbaum, C. Price, "Analysis of temperature influences on the amplitude-frequency characteristics of Rn gas concentration," *Journal of Environmental Radioactivity*, vol. 86, pp. 251-270, 2006.
- [26] R. Fujiyoshi, K. Sakamoto, T. Imanishi, T. Sumiyoshi, S. Sawamura, J. Vaupotic, J. Kobal, "Meteorological parameters contributing to variability in  $rn^{222}$  activity concentrations in soil gas at a site in Sapporo, Japan," *Science of the Total Environment*, vol. 370, pp. 224-234, 2006.
- [27] G. Prasad, Y. Prasad, G. Gusain, R. Ramola, "Measurement of radon and thoron levels in soil, water and indoor atmosphere of Budhakedar in Garhwal Himalaya, India," *Radiation Measurements*, vol. 43, pp. 375-379, 2008.
- [28] A. V. Sundal, V. Valen, O. Soldal, T. Strand, "The influence of meteorological parameters on soil radon levels in permeable glacial sediments," *Science of the Total Environment*, vol. 389, pp. 418-428, 2008.
- [29] A. Papoulis, *Probability, Random Variables, and Stochastic Processes*, Mc-Graw-Hill, 1991.